Jurnal Riset Sains dan Teknologi
Volume 10 No. 1, March 2026 (C.54 – C.68)
e-ISSN: 2549-9750
p-ISSN: 2579-9118

Discovery of Novel GLUT4 Inhibitors from Kawista (*Limonia Acidissima* L.) Bioactive Compounds Through in Silico Approaches

M. Artabah Muchlisin[1,2], Engrid Juni Astuti[*1,3], Aura Lintang Ayu Cahyani[1], Felia Rahma Cahya Andita[1], Nur Islami Vikri Abdillah[1], Aghnia Fuadatul Inayah[1,4], Taufik Muhammad Fakih[5]

[1]Department of Pharmacy, Faculty of Health Sciences, University of Muhammadiyah Malang, Malang, Indonesia
[2]Laboratory of Chemistry, University of Muhammadiyah Malang, Malang, Indonesia
[3]Central Laboratory, University of Muhammadiyah Malang, Malang, Indonesia
[4]Department of Apothecary Program, Faculty of Health Sciences, University of Muhammadiyah Malang, Malang, Indonesia
[5]Department of Pharmacy, Faculty of Mathematics and Natural Sciences, Universitas Islam Bandung, Bandung, Indonesia

*Corresponding author: engridjuni81@umm.ac.id

DOI:
10.30595/jrst.v10i1.28366

Article information:
Received:
01/10/2025

Revised:
21/12/2025

Accepted:
03/02/2026

ABSTRAK

GLUT4 (Glucose Transporter Type 4) is a key regulator of glucose homeostasis in muscle and adipose tissues. Although inhibition of GLUT4 may exacerbate hyperglycemia in diabetes, it represents a potential therapeutic strategy in cancer by limiting glucose uptake in cells reliant on aerobic glycolysis (the Warburg effect). Natural secondary metabolites are promising candidates for modulating GLUT4 activity. This study aimed to identify potential GLUT4 inhibitors from bioactive compounds of Limonia acidissima (kawista) using in silico approaches. Secondary metabolites of kawista were screened for ADMET properties and oral bioavailability. Molecular docking was performed against the cryo-EM structure of GLUT4 (PDB ID: 7WSM), followed by 200 ns molecular dynamics simulations for the top-ranked ligands. Structural stability was evaluated using RMSD, RMSF, radius of gyration (Rg), and solvent-accessible surface area (SASA). Binding free energies were calculated using the MM-PBSA method. Docking analysis showed that the native ligand cytochalasin B exhibited strong binding affinity (−9.13 kcal/mol, Ki 202.26 nM). Among 43 kawista metabolites, stigmasterol (−8.6 kcal/mol, Ki 494.04 nM) and lupeol (−7.91 kcal/mol, Ki 1.58 μM) demonstrated the most favorable binding affinities. Molecular dynamics simulations revealed stable protein–ligand complexes, with RMSD values ranging from 2.0 to 3.5 Å. RMSF analysis indicated stable key binding residues (Gln298, Gln299, Asn304, Gly400, Trp428, and Asn427), except for Trp404, which showed higher fluctuation in the lupeol complex. Rg and SASA values remained relatively constant, indicating compact and stable complexes. MM-PBSA analysis confirmed that stigmasterol exhibited the most favorable binding free energy, closely comparable to cytochalasin B. These findings suggest that stigmasterol and lupeol from Limonia acidissima are promising GLUT4 inhibitors, with stigmasterol demonstrating the most stable interaction and favorable binding profile. This study highlights the potential of kawista-derived metabolites as lead

compounds for further development of GLUT4-targeted anticancer agents.

Keywords: (GLUT4, in silico, Limonia acidissima, molecular docking, molecular dynamic

1. INTRODUCTION

GLUT4 (Glucose Transporter Type 4) is a facilitative glucose transporter predominantly expressed in adipose tissue and skeletal muscle, playing a crucial role in glucose homeostasis. Upon insulin stimulation, GLUT4 translocates to the plasma membrane to enable glucose uptake into cells (van Gerwen et al., 2023). Dysregulation of GLUT4 activity or expression impairs glucose transport and is strongly associated with the development of insulin resistance and type 2 diabetes (Zhao et al., 2023). In addition to its role in metabolic disorders, GLUT4 has also been implicated in obesity, where it contributes to lipid accumulation (Chandrasekaran & Weiskirchen, 2024). Conversely, certain types of cancer (malignant pancreatic tumors, adenocarcinoma, colon cancer, ovarian tumor cells, gliumo tumor, lymphoma, and multiple myeloma) exhibit increased GLUT4 expression to support their high glucose demand (Szablewski, 2022).

While most therapeutic strategies focus on enhancing GLUT4 activity to improve glycemic control in diabetes (Flores-Opazo et al., 2020; Zhou et al., 2016), GLUT4 inhibition holds distinct biological significance (Wei et al., 2017). In cancer, increased GLUT4 expression is often linked to the Warburg effect—a metabolic reprogramming in which tumor cells preferentially rely on aerobic glycolysis despite oxygen availability (Zhong et al., 2022). Inhibiting GLUT4 in this context may reduce glucose supply to tumor cells, thereby limiting their growth and proliferation (Pliszka & Szablewski, 2021). Additionally, suppressing GLUT4 activity in adipose tissue may help reduce lipid accumulation, suggesting potential utility in obesity management (Fang et al., 2017).

Our previous studies have suggested that *Limonia acidissima* (kawista) bioactive compounds are involved in pathways related to diabetes and cancer, including response to insulin, insulin resistance, pathways in cancer, and apoptosis, as identified through network pharmacology analysis(Hentu et al., 2024; Wahyuni et al., 2024). These pathway associations provide a mechanistic rationale for investigating kawista metabolites as potential modulators of GLUT4, a central regulator linking metabolic dysregulation and cancer-associated glucose dependence. An *in vitro* study reported that a specific fruit fraction of kawista suppressed the proliferation of human breast cancer cell lines, including SKBR3 and MDA-MB435, partly through G2/M phase cell cycle arrest (Pradhan et al., 2012). In line with these findings, an *in vivo* study demonstrated that the methanolic extract of kawista fruits significantly inhibited tumor development in Dalton ascitic lymphoma–induced mice (Eluru et al., 2015). Furthermore, another *in vivo* study showed that the ethanolic fruit extract of kawista exerted antitumor activity in Ehrlich ascites carcinoma–bearing mice (Narayanasamy et al., 2013).

In silico methods offer an efficient platform for the exploration of bioactive compounds as GLUT4 inhibitors, including molecular interaction profiling through molecular docking and stability evaluation via molecular dynamics simulations (Fakih et al., 2021). Previous studies have demonstrated the successful application of in silico modeling in identifying GLUT4-selective inhibitors for cancer therapy, highlighting its utility in structure-based drug design despite the absence of a full crystal structure for GLUT4 (Mishra et al., 2015). Recently, the availability of the cryo-EM structure of human GLUT4 (PDB ID: 7WSM) has enabled more accurate structure-based analysis (Yuan et al., 2022). This advancement allows direct molecular docking and dynamics simulations using experimentally resolved GLUT4, enhancing the reliability of in silico inhibitor screening.

This study aims to evaluate kawista bioactive compounds as potential GLUT4 inhibitors through in silico approaches. The research encompasses molecular docking to assess binding affinity and interaction patterns, and molecular dynamics simulations to analyze the structural stability of ligand-GLUT4 complexes under dynamic conditions.

Table 1. The list of secondary metabolites of kawista

No.	Compound Code	Compound Name	SMILES	Pubchem ID
1	Mol1	Bergapten	COC1=C2C=CC(=O)OC2=CC3=C1C=CO3	2355
2	Mol2	Demethylsuberosin	CC(=CCC1=C(C=C2C(=C1)C=CC(=O)O2)O)C	5316525
3	Mol3	Isopimpinellin	COC1=C2C=COC2=C(C3=C1C=CC(=O)O3)OC	68079
4	Mol4	Osthenol	COC1=C2C=COC2=C(C3=C1C=CC(=O)O3)OC	5320318
5	Mol5	Psoralen	C1=CC(=O)OC2=CC3=C(C=CO3)C=C21	6199
6	Mol6	Xanthotoxin	COC1=C2C(=CC3=C1OC=C3)C=CC(=O)O2	4114
7	Mol7	Gallocatechin	C1[C@@H]([C@H](OC2=CC(=CC(=C21)O)O)C3=CC(=C(C(=C3)O)O)O)O	65084
8	Mol8	Saponarin	C1=CC(=CC=C1C2=CC(=O)C3=C(C(=C(C=C3O2)O[C@H]4[C@@H]([C@H]([C@@H]([C@H](O4)CO)O)O)O)[C@H]5[C@@H]([C@H]([C@@H]([C@H](O5)CO)O)O)O)O)O	441381
9	Mol9	Vitexin	C1=CC(=CC=C1C2=CC(=O)C3=C(O2)C(=C(C=C3O)O)[C@H]4[C@@H]([C@H]([C@@H]([C@H](O4)CO)O)O)O)O	5280441
10	Mol10	Gallic acid	C1=C(C=C(C(=C1O)O)O)C(=O)O	370
11	Mol11	4-Hydroxybenzoic acid	C1=CC(=CC=C1C(=O)O)O	135
12	Mol12	Acidissiminol	CC(=CCC(/C(=C/COC1=CC=C(C=C1)CCNC(=O)C2=CC=CC=C2)/C)O)C	14506785
13	Mol13	Acidissiminol epoxide	C/C(=C\COC1=CC=C(C=C1)CCNC(=O)C2=CC=CC=C2)/C(CC3C(O3)(C)C)O	5363185
14	Mol14	Dihydroxyacidissiminol	C/C(=C\COC1=CC=C(C=C1)CCNC(=O)C2=CC=CC=C2)/C(CC(C(C)(C)O)O)O)O	101676196
15	Mol15	N-benzoyltyramine	C1=CC=C(C=C1)C(=O)NCCC2=CC=C(C=C2)O	577614
16	Mol16	Acidissimin	CCCCCCCCCCCCCCCCCC(=O)OC(CC=C(C)C)/C(=C/COC1=CC=C(C=C1)CCNC(=O)C2=CC=CC=C2)/C	6442730
17	Mol17	Suberenol	CC(C)(/C=C/C1=C(C=C2C(=C1)C=CC(=O)O2)OC)O	5375166
18	Mol18	Columbianetin	CC(C)([C@@H]1CC2=C(O1)C=CC3=C2OC(=O)C=C3)O	92201
19	Mol19	Limodissimin A	CC(=C)[C@@H](CC1=C(C=CC2=C1OC(=O)C=C2)OC3=CC4=C(C=C3)C=CC(=O)O4)O	163183899
20	Mol20	Marmesin	CC(C)([C@@H]1CC2=C(O1)C=C3C(=C2)C=CC(=O)O3)O	334704
21	Mol21	Seselin	CC1(C=CC2=C(O1)C=CC3=C2OC(=O)C=C3)C	68229
22	Mol22	Syringaldehyde	COC1=CC(=CC(=C1O)OC)C=O	8655
23	Mol23	Syringaresinol	COC1=CC(=CC(=C1O)OC)C2C3COC(C3CO2)C4=CC(=C(C(=C4)OC)O)OC	100067
24	Mol24	Yangambin	COC1=CC(=CC(=C1OC)OC)[C@@H]2[C@H]3CO[C@@H]([C@H]3CO2)C4=CC(=C(C(=C4)OC)OC)OC	443028
25	Mol25	Physcion	CC1=CC2=C(C(=C1)O)C(=O)C3=C(C2=O)C=C(C=C3O)OC	10639
26	Mol26	3-Formylindole	C1=CC=C2C(=C1)C(=CN2)C=O	10256
27	Mol27	4-Methoxy-1-methyl-2-quinolone	CN1C2=CC=CC=C2C(=CC1=O)OC	182073
28	Mol28	4-Methoxy-2-quinolone	COC1=CC(=O)NC2=CC=CC=C21	600167
29	Mol29	Edulitine	COC1=CC=CC2=C1NC(=O)C=C2OC	826073
30	Mol30	N, N-dimethyltryptamine	CN(C)CCC1=CNC2=CC=CC=C21	6089
31	Mol31	Tanakamine	CC(C)(C(CO)C1=CNC2=CC=CC=C21)O	101417302
32	Mol32	Tanakine	CC(C)(C(CC1=CNC2=CC=CC=C21)O)O	57357311
33	Mol33	Tembamide	COC1=CC=C(C=C1)C(CNC(=O)C2=CC=CC=C2)O	177583
34	Mol34	Hederatriol	C[C@]12CC[C@@H]([C@@](C1CC[C@@]3(C2CC=C4[C@]3(CC[C@@]5([C@H]4CC(CC5)(C)C)CO)C)C)(C)CO)O	44144287
35	Mol35	Limonin	C[C@@]12CC[C@H]3[C@]([C@@]14[C@H](O4)C(=O)O[C@H]2C5=COC=C5)(C(=O)C[C@@H]6[C@@]37COC(=O)C[C@@H]7OC6(C)C)C	179651
36	Mol36	Lupeol	CC(=C)[C@@H]1CC[C@]2([C@H]1[C@H]3CC[C@@H]4[C@]5(CC[C@@H](C([C@@H]5CC[C@]4([C@@]3(CC2)C)C)(C)C)O)C)C	259846
37	Mol37	Obacunone	C[C@@]12CC[C@@H]3[C@]4(C=CC(=O)OC([C@@H]4CC(=O)[C@]3([C@@]15[C@H](O5)C(=O)O[C@H]2C6=COC=C6)C)(C)C)C	119041
38	Mol38	Rutaevin	C[C@@]12CC[C@H]3[C@]([C@@]14[C@H](O4)C(=O)O[C@H]2C5=COC=C5)([C@H](C(=O)[C@@H]6[C@@]37COC(=O)C[C@@H]7OC6(C)C)O)C	441805
39	Mol39	Stigmasterol	CC[C@H](/C=C/[C@@H](C)[C@H]1CC[C@@H]2[C@@]1(CC[C@H]3[C@H]2CC=C4[C@@]3(CC[C@@H](C4)O)C)C)C(C)C	5280794
40	Mol40	Orientin	C1=CC(=C(C=C1C2=CC(=O)C3=C(O2)C(=C(C=C3O)O)[C@H]4[C@@H]([C@H]([C@@H]([C@H](O4)CO)O)O)O)O)O	5281675
41	Mol41	Aurapten	CC(=CCC/C(=C/COC1=CC2=C(C=C1)C=CC(=O)O2)/C)C	1550607
42	Mol42	Dihydrosuberenol	CC(C)(CCC1=C(C=C2C(=C1)C=CC(=O)O2)OC)O	14077805
43	Mol43	Osthol	CC(=CCC1=C(C=CC2=C1OC(=O)C=C2)OC)C	10228

2. MATERIAL AND METHODS

2.1 Preparation of ligand structure

The kawista's bioactive compounds was obtained from literature (Murthy & Dalawai, 2020) and then screening and searching for the structure from PubChem database (https://pubchem.ncbi.nlm.nih.gov) (Table 1). The compounds was prepared for 3D structure with Avogadro 1.2.0 (Hanwell et al., 2012) and geometry optimization with GFN.xTB (Bannwarth et al., 2019).

2.2 Preparation of macromolecules

The crystallographic structure of GLUT4 bound to cytochalasin B, a known GLUT inhibitor (Temre et al., 2022), as native ligand (PDB ID: 7WSM) was obtained from Protein Data Bank (https:// www.rcsb.org) (Yuan et al., 2022). GLUT4 was separated from native ligand using Biovia Studio Visualizer v21.1.0.20298 (Dassault Systèmes, 2020) and save each in pdb format.

2.3 Molecular docking simulations

Molecular docking simulation was carried out using PyRx 0.8 with AutoDock 4.2.1 protocols (Dallakyan & Olson, 2015). Kawista's bioactive compounds and native ligand was docked GLUT4 at initial position with 10 points size and 1 Å space of grid box (x = 94.164; y = 98.065; z = 101.550). The docking protocols was run with 100 Lamarckian Genetic Algorithm conformation runs (Anggraeni et al., 2023). Validation of this protocal was done by re-docking the native ligand to GLUT4. The protocal was declared valid if have RMSD values <2 Å (Anggraeni et al., 2023). The docking pose with lowest free binding energy (ΔG) in most favoured cluster was chosen as the best docking pose (Muchtaridi et al., 2018). The protein-ligand complexes from the docking simulation were visualized using ProteinsPlus (Schöning-Stierand et al., 2022). The two compound with lowest docking score would proceed to next step.

2.4 Molecular dynamics simulations

Molecular dynamics simulations were performed on GROMACS v2024.2 using AMBER99SB-ILDN force field (Hikmawati et al., 2022). The simulation was employed for 200 ns with 10 ps timestep. The TIP3P water cube model was used on solvation of system (Mark & Nilsson, 2001), and neutralization was carried out by adding Na^+ and Cl^- ions. Furthermore, analysis of the root-mean-square deviation (RMSD), root-mean-square fluctuation (RMSF), radius of gyration (Rg), and solvent-accessible surface area (SASA) as well as principal component analysis (PCA) were conducted to evaluate the system stability of the complexes.

3. RESULTS AND DISCUSSION

3.1 Molecular docking simulations

Molecular docking analysis was performed to evaluate the binding affinity of secondary metabolites from *Limonia acidissima* against GLUT4 (PDB ID: 7WSM). Re-docking of native ligand to GLUT4 protein showed good result with RMSD (0.49-0.66 Å) from 100 runs. Native ligand exhibited a ΔG of –9.13 kcal/mol and a predicted inhibition constant (Ki) of 202.26 nM (Table 2), confirming its high affinity for GLUT4. Among the tested compounds, mol39 demonstrated the strongest binding affinity, with a ΔG of –8.60 kcal/mol and a predicted Ki of 494.04 nM, and followed by mol36, with a ΔG of –7.91 kcal/mol and a predicted Ki of 1.58 μM.

From the interaction perspective, the native ligand formed four hydrogen bonds with amino acid residues Gln298, Gln299, Gly400, and Trp404, and two hydrophobic interactions with Gln177 and Trp404. Mol15 shared three hydrogen bonds with the native ligand (Gln298, Gln299, and Trp404) but did not share any hydrophobic interactions. Mol12 and Mol19 shared two hydrogen bonds (Gln298 and Trp404) and conserved all hydrophobic interactions observed in the native ligand. Mol36 and Mol39, which exhibited the best docking scores, shared a common hydrophobic interaction with Trp404 that was also present in the native ligand, indicating binding within the same pocket. Unlike the native ligand, both compounds formed only a single hydrogen bond with Glu396 and relied predominantly on hydrophobic interactions for stabilization, as evidenced by the increased number of hydrophobic contacts relative to hydrogen bonds, which contributes favorably to ΔG in docking scoring functions.

Table 2. The molecular docking result of secondary metabolite of kawista to GLUT4

No.	Compound Code	ΔG (Kcal/mol)	Predicted *Ki*
1	Mol1	-5.2	154,39 µM
2	Mol2	-5.2	154,03 µM
3	Mol3	-4.92	246,57 µM
4	Mol4	-5.35	120.11 µM
5	Mol5	-4.98	222.02 µM
6	Mol6	-4.58	441.97 µM
7	Mol7	-4.07	1.71 mM
8	Mol8	+69712.28	-
9	Mol9	-4.75	329.99 µM
10	Mol10	-2.53	13.96 mM
11	Mol11	-2.99	6.46 mM
12	Mol12	-5.49	95.01 µM
13	Mol13	-5.44	102.38 µM
14	Mol14	-4.65	389.21 µM
15	Mol15	-5.19	155.96 µM
16	Mol16	+12.12	-
17	Mol17	-5.70	66.67 µM
18	Mol18	-4.99	219.29 µM
19	Mol19	-6.31	23.77 µM
20	Mol20	-5.76	59.55 µM
21	Mol21	-5.34	122.81 µM
22	Mol22	-3.45	2.98 mM
23	Mol23	-3.75	1.79 mM
24	Mol24	-2.90	7.46 mM
25	Mol25	-5.86	50.55 µM
26	Mol26	-3.79	1.65 mM
27	Mol27	-4.55	458.77 µM
28	Mol28	-4.05	1.07 mM
29	Mol29	-4.21	822.68 µM
30	Mol30	-3.53	2.58 mM
31	Mol31	-3.32	3.68 mM
32	Mol32	-4.20	833.17 µM
33	Mol33	-4.63	401.14 µM
34	Mol34	+4.73	-
35	Mol35	-5.3	129.36 µM
36	Mol36	-7.91	1.58 µM
37	Mol37	-7.27	4.71 µM
38	Mol38	-5.86	50.58 µM
39	Mol39	-8.6	494.04 nM
40	Mol40	-4.35	650.14 µM
41	Mol41	-5.72	64.57 µM
42	Mol42	-5.3	129.50 µM
43	Mol43	-5.08	350.12 µM
44	Cytochalasin B	-9.13	202.26 nM

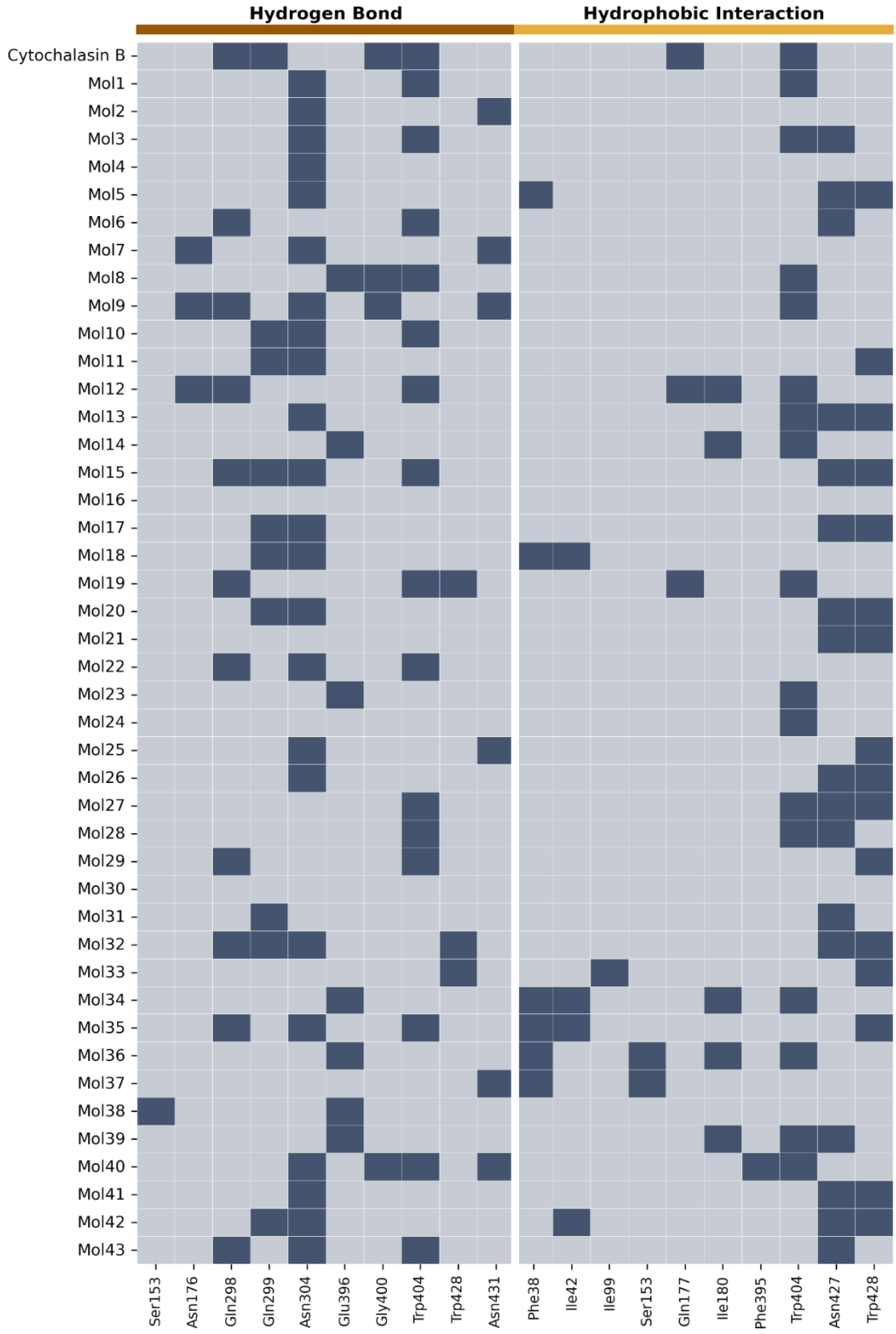

Figure 1. Hydrogen bond and hydrophobic interaction profiles obtained from docking. Dark grey indicates interaction, whereas light grey indicates no interaction.

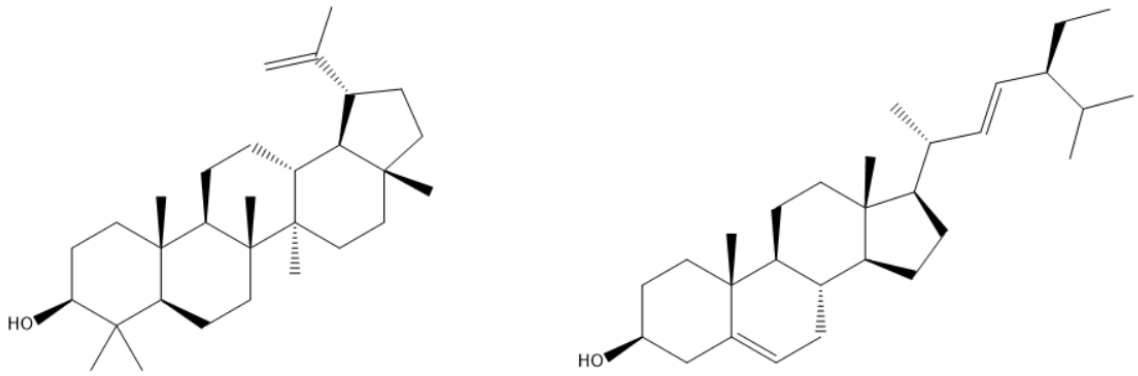

Figure 2. The structure of mol36 (left) and mol39 (right)

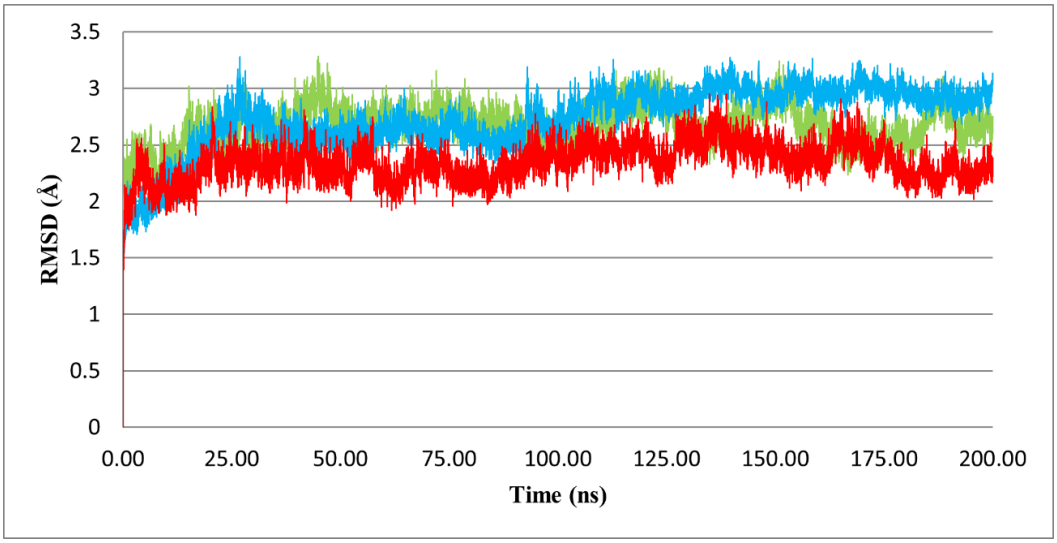

Figure 3. The RMSD of native (green), mol39 (blue), and mol36 (red) during 200 ns simulation

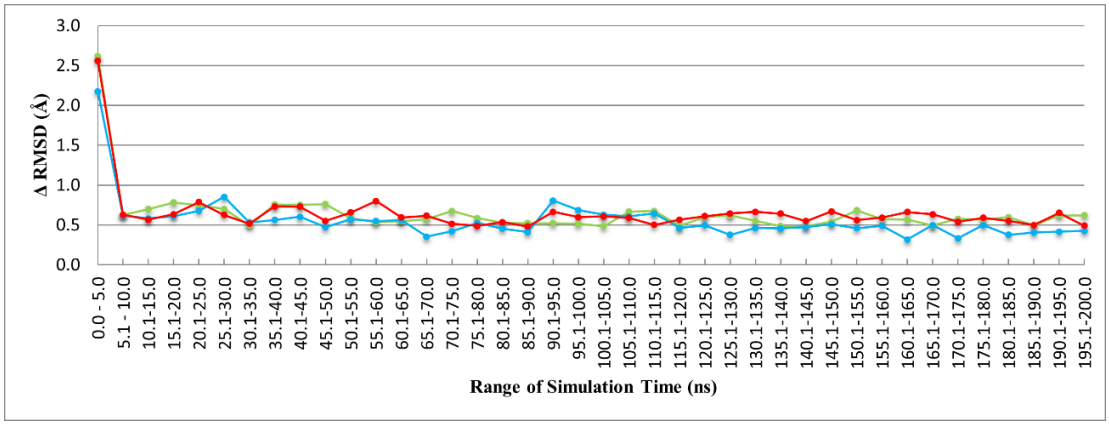

Figure 4. The average RMSD (Δ RMSD) in every 5 ns simulation of native (green), mol39 (blue), and mol36 (red)

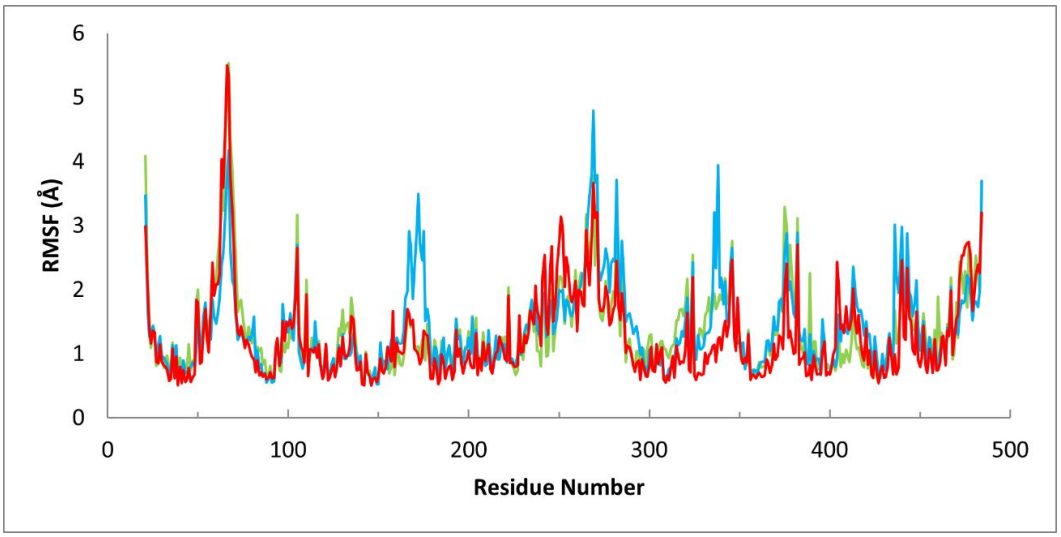

Figure 5. The RMSF plot of native (green), mol39 (blue), and mol36 (red)

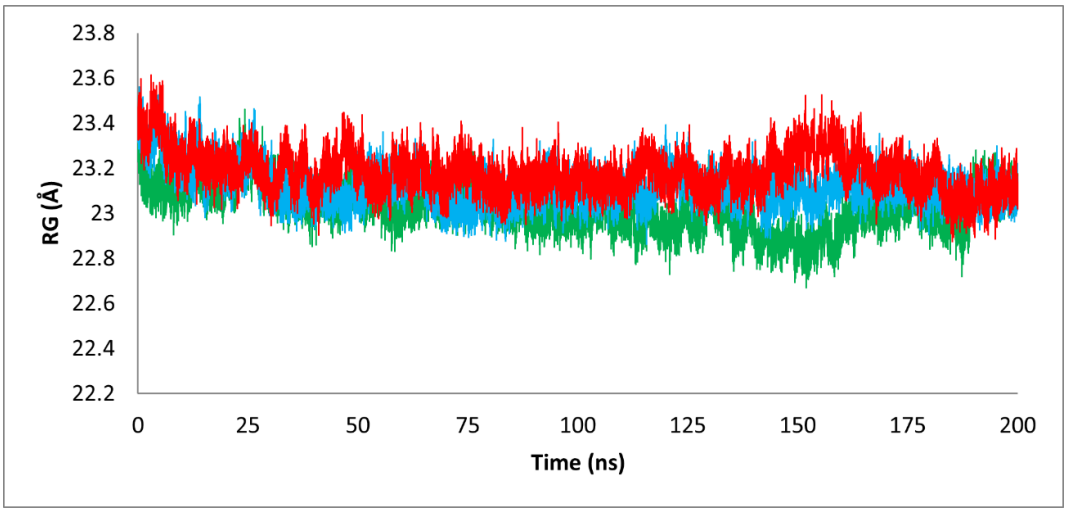

Figure 6. The Rg of native (green), stigmasterol (blue), and limonin (red) during 200 ns simulation

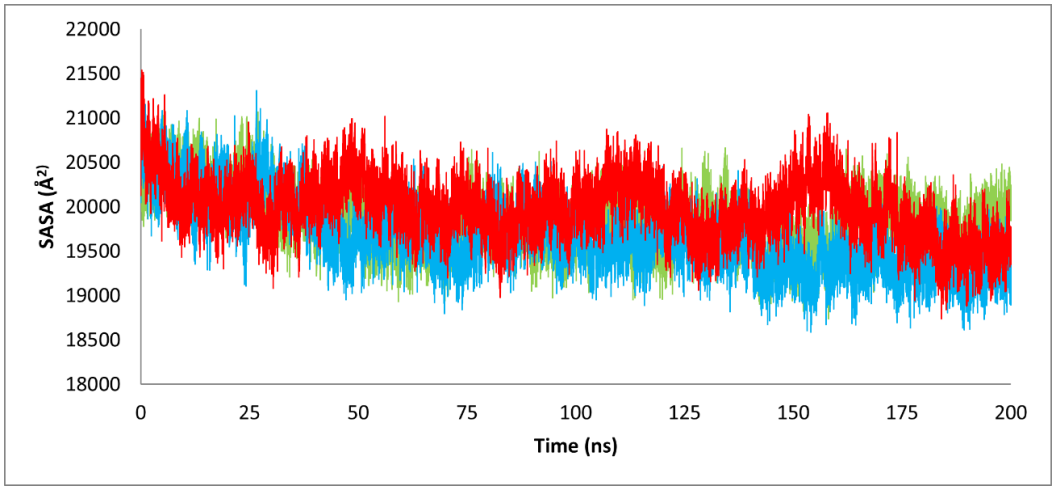

Figure 7. The SASA of native (green), stigmasterol (blue), and limonin (red) during 200 ns simulation

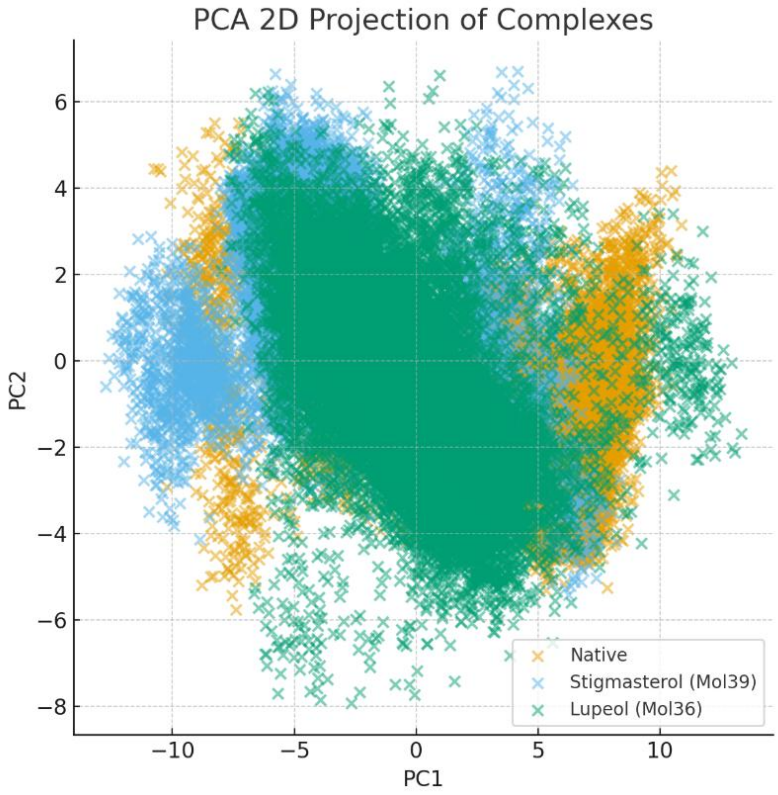

Figure 8. PCA 2D projection plot of complexes

3.2 Molecular dynamic simulations

Molecular dynamics simulations for 200 ns were performed to evaluate the stability of GLUT4 complexes with the native ligand, Mol39, and Mol36. The observed average RMSD values exceeding 2 Å (Figure 3) for all GLUT4–ligand complexes are consistent with the structural and dynamic characteristics of the GLUT4 transporter and the simulation setup. GLUT4 is a multi-pass transmembrane protein that exhibits intrinsic conformational flexibility during substrate binding and transport (Bai & Li, 2023; Thomas et al., 2023). Membrane transporters undergo substantial conformational rearrangements during their functional cycle, including transitions between outward-facing and inward-facing states. These transitions involve collective movements of transmembrane helices and loop regions, which commonly result in higher RMSD values in molecular dynamics simulations (Garaeva & Slotboom, 2020; Liu et al., 2016). Previous MD studies on transmembrane proteins have reported RMSD values above 2 Å while maintaining structural stability. For example, the UlaA transporter in *Escherichia coli* reached equilibrium with RMSD values ranging from 5.8 to 6.7 Å (Faghih-Mirzaee et al., 2017). Similarly, simulations of the sarcolipin pentamer embedded in a POPC membrane showed RMSD convergence at approximately 3.2–3.5 Å after 120 ns, indicating a stable yet dynamically flexible transmembrane assembly (Cao et al., 2015).

RMSD analysis in the present study showed that all three GLUT4–ligand complexes experienced an initial increase in structural deviation during the early equilibration phase (0–20 ns), followed by stabilization for the remainder of the simulation. To further assess short-term stability, average RMSD changes (ΔRMSD) calculated at 5 ns intervals were analyzed. ΔRMSD refers to the change in RMSD values over time or between different states of a molecular system. It can indicate conformational changes and stability (Alwash et al., 2025). The ΔRMSD values for all complexes remained within <1 Å (Figure 4). A low ΔRMSD value indicates that the structures are similar and stable over time, while a high ΔRMSD suggests greater conformational variability and potential instability (Malau & Sianturi, 2017).

Table 3. The RMSF value of GLUT4 key residue is about 6 Å from native

Residue Number	Native	Mol39	Mol36
Phe38	0.922	1.130	0.953
Ile42	0.882	0.891	0.743
Ser96	0.719	0.859	0.975
Ile99	1.167	1.500	1.496
Gly150	0.664	0.524	0.624
Ser153	0.780	0.887	0.689
Gly154	0.800	0.875	0.800
Pro157	0.772	1.216	0.880
Asn176	0.894	1.507	1.303
Gln177	1.469	1.695	1.283
Ile180	0.880	0.813	0.607
Val181	1.214	1.108	0.924
Ile184	0.856	0.973	0.594
Gln295	0.652	0.983	0.594
Gln298	0.779	0.785	0.647
Gln299	1.068	0.659	0.642
Ile303	0.799	0.717	0.721
Asn304	1.080	1.146	1.145
Phe307	1.195	1.100	1.093
Tyr308	1.094	0.666	0.602
Asn333	1.881	1.332	0.982
Phe395	0.727	0.662	0.680
Glu396	1.421	1.537	1.018
Pro399	0.836	0.678	0.705
Gly400	0.744	0.719	0.673
Pro401	0.826	0.831	0.787
Trp404	0.857	0.934	2.427
Ala423	0.674	0.959	0.666
Gly424	0.619	0.807	0.626
Phe425	0.983	1.266	1.037
Asn427	0.572	0.676	0.540
Trp428	0.658	0.614	0.705
Average RMSF	0.921	0.970	0.880

Table 4. The results of MM/PBSA

Energy	Native	Mol39	Mol36
Δvan der Waal energy	-65.02 ± 3.93 kcal/mol	-61.87 ± 5.10 kcal/mol	-55.02 ± 2.93 kcal/mol
ΔElectrostattic energy	-2.69 ± 2.71 kcal/mol	-2.05 ± 2.12 kcal/mol	-0.69 ± 0.81 kcal/mol
ΔPolar solvation energy	28.37 ± 3.77 kcal/mol	24.86 ± 2.69 kcal/mol	25.37 ± 3.78 kcal/mol
ΔSASA energy	-6.42 ± 0.19 kcal/mol	-5.93 ± 0.19 kcal/mol	-5.44 ± 0.19 kcal/mol
ΔBinding energy	-45.76 ± 4.04 kcal/mol	-44.99 ± 4.93 kcal/mol	-35.78 ± 4.04 kcal/mol

Among the tested ligands, Mol39 exhibited slightly higher RMSD fluctuations compared to Mol36, reflecting more dynamic protein–ligand interactions, whereas Mol36 showed lower average RMSD and reduced fluctuations, suggesting a stabilizing effect on the GLUT4 structure.

To further investigate the stability of interactions between GLUT4 and each ligand, residue fluctuation (RMSF) analysis was performed on key residues involved in hydrogen bonding and hydrophobic interactions (Figure 5). The results showed that almost all critical residues, such as Gln298, Gln299, Asn304, Gly400, Trp428, and Asn427, exhibited RMSF values below 1.5 Å in all three complexes, indicating high local structural stability during the 200 ns simulation (Table 3).

Gln299, which plays a role in hydrogen bonding, showed very low RMSF values in complexes with mol39 (0.659 Å) and mol36 (0.642 Å), lower than that of the native ligand (1.068 Å). Trp404, a key residue involved in both hydrogen bonding and hydrophobic interactions, was highly stable in the native ligand and mol39 complexes (RMSF ~0.85–0.93 Å), but displayed significant fluctuation in the mol36 complex (2.427 Å). This suggests a possible shift in binding or weaker interaction between lupeol and the active site of GLUT4.

Other residues that consistently remained stable across all complexes, such as Ile42, Ile180, Gln298, and Gly400, indicate that the binding domain of GLUT4 was structurally maintained in the presence of any ligand. However, the mol39 complex showed a fluctuation pattern most similar to the native ligand, whereas mol36, although more stable overall (RMSD), experienced local instability at the critical residue Trp404.

Rg was analyzed to assess complex stability between folded and unfolded states. Lower Rg suggests greater stability in conformation (Hikmawati et al., 2022). SASA provided additional insight into ligand–protein stability. SASA offer a quantitative assessment of the surface area exposed to solvent (Wang et al., 2020). PCA was performed to evaluate protein–ligand fluctuations, with eigenvector direction and amplitude examined through 2D trajectory projections to characterize complex dynamics (Pitaloka et al., 2021).

The Rg analysis (Figure 6) indicated that the native ligand complex exhibited a more compact conformation (average Rg = 23.02 Å, range = 22.67–23.46 Å) compared with Mol36 (23.61 Å; 22.88–23.61 Å) and Mol39 (23.56 Å; 22.86–23.56 Å). The narrower range of the native complex suggests lower structural fluctuations, reflecting higher overall stability. In contrast, Mol36 showed the widest range, implying greater flexibility during the simulation, while Mol39 displayed intermediate behavior. Notably, the Rg values of all complexes converged at the end of the 200 ns simulation (native = 23.06 Å, Mol36 = 23.11 Å, Mol39 = 23.05 Å), indicating that despite minor differences, all systems maintained a stable folded state without significant unfolding events.

SASA analysis (Figure 7) revealed that the native complex maintained an average solvent-accessible surface area of 19,850.2 $Å^2$ (range: 18,741.9–21,092.8 $Å^2$), whereas Mol39 and Mol36 exhibited averages of 19,663.9 $Å^2$ (18,589.9–21,307.2 $Å^2$) and 19,982.6 $Å^2$ (18,742.3–21,538.3 $Å^2$), respectively. Mol39 showed the lowest average SASA, suggesting a slightly more compact conformation, although its wide fluctuation range indicated transient structural expansions. Mol36 demonstrated the highest average SASA with the broadest range, reflecting greater conformational flexibility and solvent exposure. In comparison, the native complex displayed a balanced profile, characterized by moderate SASA values and narrower fluctuations, consistent with higher structural stability during the simulation.

PCA plots (Figure 8) showed that the native complex formed a compact cluster, reflecting high structural stability. Mol39 displayed moderate dispersion, suggesting intermediate stability, whereas Mol36 exhibited the widest spread, indicating greater conformational flexibility and conformational variability compared with the other systems.

The MM/PBSA binding free energy calculations (Table 4) revealed that the native complex exhibited the strongest binding affinity (−45.76 ± 4.04 kcal/mol), followed closely by mol39 with −44.99 ± 4.93 kcal/mol, whereas mol36 showed considerably weaker binding (−35.78 ± 4.04 kcal/mol). Van der Waals interactions were the primary driving force for complex stabilization, with the native complex showing the most favorable contribution (−65.02 ± 3.93 kcal/mol).

Electrostatic interactions also favored the native complex (−2.69 ± 2.71 kcal/mol) over mol39 and mol36. Although polar solvation energies opposed binding in all systems, they were particularly high in the native complex (28.37 ± 3.77 kcal/mol). Nevertheless, the non-polar solvation (ΔSASA) contribution further stabilized the native complex (−6.42 ± 0.19 kcal/mol). Overall, these results suggest that the native ligand remains the most stable binder, with mol39 providing a comparable alternative, while mol36 demonstrates substantially weaker binding affinity.

3. CONCLUSION

Based on molecular docking and molecular dynamics analyses, Stigmasterol (Mol39) demonstrated better interaction stability compared to Lupeol (Mol36). PCA results indicated that the Mol39 complex was more compact and stable throughout the simulation than Mol36. The Δbinding energy analysis further supported this finding, showing that Mol39 (−44.99 ± 4.93 kcal/mol) was close to the native ligand (−45.76 ± 4.04 kcal/mol), whereas Mol36 exhibited weaker binding energy (−35.78 ± 4.04 kcal/mol). Therefore, Stigmasterol shows greater potential as a candidate GLUT4 inhibitor compared to Lupeol.

ACKNOWLEDGEMENT

The authors thanks to LPPI University of Muhammadiyah Malang for funding this research.

REFERENCES

Alwash, A. H., Yaseen, Y. S., Najumuldeen, Z., & Ibrahim, N. K. (2025). In Silico Profiling of New 1,2,3,4-Tetrahydropyrimidine Derivatives Linked to Hydroxamate Moiety by Various Aromatic Linkers as HDACs Inhibitors. *Advanced Journal of Chemistry, Section A*, *8*(7), 1201–1223. https://doi.org/10.48309/AJCA.2025.469784.1612

Anggraeni, A. D., Putri, N. Y. F., Amalia, S. D., & Muchlisin, M. A. (2023). Bioavailability and Molecular Docking Prediction of Secondary Metabolite of Curcuma zedoaria as Potential MPRO SARS COV-2 Inhibitor. *Medical Sains : Jurnal Ilmiah Kefarmasian*, *8*(4), 1345–1354. https://doi.org/10.37874/ms.v8i4.805

Bai, L., & Li, H. (2023). Structural insights into the membrane chaperones for multi-pass membrane protein biogenesis. *Current Opinion in Structural Biology*, *79*(102563). https://doi.org/10.1016/j.sbi.2023.102563

Bannwarth, C., Ehlert, S., & Grimme, S. (2019). GFN2-xTB - An Accurate and Broadly Parametrized Self-Consistent Tight-Binding Quantum Chemical Method with Multipole Electrostatics and Density-Dependent Dispersion Contributions. *Journal of Chemical Theory and Computation*, *15*(3), 1652–1671. https://doi.org/10.1021/acs.jctc.8b01176

Cao, Y., Wu, X., Lee, I., & Wang, X. (2015). Molecular dynamics of water and monovalent-ions transportation mechanisms of pentameric sarcolipin. *Proteins: Structure, Function, and Bioinformatics*, *84*(1), 73–81. https://doi.org/10.1002/prot.24956

Chandrasekaran, P., & Weiskirchen, R. (2024). The Role of Obesity in Type 2 Diabetes Mellitus—An Overview. *International Journal of Molecular Sciences*, *25*(1882). https://doi.org/10.3390/ijms25031882

Dallakyan, S., & Olson, A. J. (2015). Small Molecule Library Screening by Docking with PyRx. *Methods in Molecular Biology*, *1263*, 243–250.

Dassault Systèmes. (2020). *Biovia Discovery Studio 2021* (v21.1.0.20298). Dassault Systèmes.

Eluru, J. R., Taranalli, A. D., & Kawatra, S. (2015). Anti-Tumour Activity of Limonia acidissima L . Methanolic Extract in Mice Model of Dalton ' s Ascitic Lymphoma. *International Journal of Pharmacognosy and Phytochemical Research*, *7*(6), 1094–1100.

Faghih-Mirzaee, E., Dehestani, M., & Zeidabadinejad, L. (2017). Computational study on transfer of L-ascorbic acid by UlaA through Escherichia coli membrane. *Journal of Bioinformatics and Computational Biology*, *15*(3), 1750007.

https://doi.org/10.1142/S021972001750007X

Fakih, T. M., Wisnuwardhani, H. A., Dewi, M. L., Ramadhan, D. S. F., Hidayat, A. F., & Prayitno, R. (2021). Simulasi Dinamika Molekuler Senyawa Asam Ferulat dan Turunannya dari Kulit Buah Nanas (Ananas comosus) sebagai Inhibitor Enzim Tirosinase. *Jurnal Sains Farmasi & Klinis*, *8*(2), 208. https://doi.org/10.25077/jsfk.8.2.208-220.2021

Fang, P., Yu, M., Zhang, L., Wan, D., Shi, M., Zhu, Y., Bo, P., & Zhang, Z. (2017). Baicalin against obesity and insulin resistance through activation of AKT/AS160/GLUT4 pathway. *Molecular and Cellular Endocrinology*, *448*, 77–86. https://doi.org/10.1016/j.mce.2017.03.027

Flores-Opazo, M., McGee, S. L., & Hargreaves, M. (2020). Exercise and GLUT4. *Exercise and Sport Sciences Reviews*, *48*(3), 110–118. https://doi.org/10.1249/JES.0000000000000224

Garaeva, A. A., & Slotboom, D. J. (2020). Elevator-type mechanisms of membrane transport. *Biochemical Society Transactions*, *48*(3), 1227–1241. https://doi.org/10.1042/BST20200290

Hanwell, M. D., Curtis, D. E., Lonie, D. C., Vandermeersch, T., Zurek, E., & Hutchison, G. R. (2012). Avogadro : an advanced semantic chemical editor , visualization , and analysis platform. *Journal of Cheminformatics*, *4*(1), 1–17. https://doi.org/10.1186/1758-2946-4-17

Hentu, D. S. R. M., Muchlisin, M. A., Jamil, A. S., Astuti, E. J., & Rafikayanti, A. (2024). Pemanfaatan Senyawa Metabolit Sekunder Kawista (Limonia acidissima) Untuk Pengelolaan Dabetes : Tinjauan Analisis Jejaring Farmakologi. *Pharma Xplore : Jurnal Sains Dan Ilmu Farmasi*, *9*(1), 51–63.

Hikmawati, D., Fakih, T. M., Sutedja, E., Dwiyana, R. F., atik, N., & Ramadhan, D. S. F. (2022). Pharmacophore-guided virtual screening and dynamic simulation of Kallikrein-5 inhibitor: Discovery of potential molecules for rosacea therapy. *Informatics in Medicine Unlocked*, *28*, 100844. https://doi.org/10.1016/j.imu.2022.100844

Liu, H., Li, D., Li, Y., & Hou, T. (2016). Atomistic molecular dynamics simulations of ATP-binding cassette transporters. *WIREs Computational Molecular Science*, *6*(3), 255–265. https://doi.org/10.1002/wcms.1247

Malau, N. D., & Sianturi, M. (2017). Molecular Dynamics Approach in Designing Thermostable Aspergillus niger Xylanase Molecular Dynamics Approach in Designing Thermostable Aspergillus niger Xylanase. In Y. W. Sari (Ed.), *IOP Conference Series: Earth and Environmental Science* (p. 012063). Institute of Physics Publishing. https://doi.org/10.1088/1755-1315/5

Mark, P., & Nilsson, L. (2001). Structure and dynamics of the TIP3P, SPC, and SPC/E water models at 298 K. *Journal of Physical Chemistry A*, *105*(43), 9954–9960. https://doi.org/10.1021/jp003020w

Mishra, R. K., Wei, C., Hresko, R. C., Bajpai, R., Heitmeier, M., Matulis, S. M., Nooka, A. K., Rosen, S. T., Hruz, P. W., Schiltz, G. E., & Shanmugam, M. (2015). In Silico Modeling-based Identification of Glucose Transporter 4 (GLUT4)-selective Inhibitors for Cancer Therapy. *Journal of Biological Chemistry*, *290*(23), 14441–14453. https://doi.org/10.1074/jbc.M114.628826

Muchtaridi, M., Dermawan, D., & Yusuf, M. (2018). Molecular docking, 3D structure-based pharmacophore modeling, and ADME prediction of alpha mangostin and its derivatives against estrogen receptor alpha. *Journal of Young Pharmacists*, *10*(3), 252–259. https://doi.org/10.5530/jyp.2018.10.58

Murthy, H. N., & Dalawai, D. (2020). Bioactive Compounds of Wood Apple (Limonia acidissima L.). In H. N. Murthy & V. A. Bapat (Eds.), *Bioactive Compounds in Underutilized Fruits and Nuts* (pp. 543–569). Springer Nature Switzerland. https://doi.org/10.1007/978-3-030-06120-3_12-1

Narayanasamy, N., Uthamaramasamy, S., Sundaravadivel, R., & Ke, P. (2013). Evaluation of Cytotoxic Effect of Limonia acidissima on. *International Journal of*

Pharmaceutical Sciences Review and Research, *19*(1), 64–68.

Pitaloka, D. A. E., Ramadhan, D. S. F., Arfan, Chaidir, L., & Fakih, T. M. (2021). Docking-Based Virtual Screening and Molecular Dynamics Simulations of Quercetin Analogs as Enoyl-Acyl Carrier Protein Reductase (InhA) Inhibitors of Mycobacterium tuberculosis. *Scientia Pharmaceutica*, *89*(20).

Pliszka, M., & Szablewski, L. (2021). Glucose transporters as a target for anticancer therapy. *Cancers*, *13*(16). https://doi.org/10.3390/cancers13164184

Pradhan, D., Tripathy, G., & Patanaik, S. (2012). Anticancer Activity of Limonia acidissima Linn (Rutaceae) Fruit Extracts on Human Breast Cancer Cell Lines. *Tropical Journal of Pharmaceutical Research*, *11*(3), 413–419. https://doi.org/10.4314/tjpr.v11i3.10

Schöning-Stierand, K., Diedrich, K., Ehrt, C., Flachsenberg, F., Graef, J., Sieg, J., Penner, P., Poppinga, M., Ungethüm, A., & Rarey, M. (2022). ProteinsPlus: a comprehensive collection of web-based molecular modeling tools. *Nucleic Acids Research*, *50*(W1), W611–W615. https://doi.org/10.1093/nar/gkac305

Szablewski, L. (2022). Glucose transporters as markers of diagnosis and prognosis in cancer diseases. *Oncology Reviews*, *16*(561). https://doi.org/10.4081/oncol.2022.561

Temre, M. K., Kumar, A., & Singh, S. M. (2022). An appraisal of the current status of inhibition of glucose transporters as an emerging antineoplastic approach: Promising potential of new pan-GLUT inhibitors. *Frontiers in Pharmacology*, *13*, 1035510. https://doi.org/10.3389/fphar.2022.1035510

Thomas, B., Chockalingam, K., & Chen, Z. (2023). Methods for Engineering Binders to Multi-Pass Membrane Proteins. *Bioengineering*, *10*(12), 1351. https://doi.org/10.3390/bioengineering10121351

van Gerwen, J., Shun-Shion, A. S., & Fazakerley, D. J. (2023). Insulin signalling and GLUT4 trafficking in insulin resistance. *Biochemical Society Transactions*, *51*(3), 1057–1069. https://doi.org/10.1042/BST20221066

Wahyuni, R. S., Muchlisin, M. A., Jamil, A. S., Astuti, E. J., & Rafikayanti, A. (2024). Integrative Network Pharmacology Unveils Limonia acidissima as a Potential Natural Product for Targeting Cancer. *Borneo Journal of Pharmacy*, *7*(3), 233–246. https://doi.org/10.33084/bjop.v7i3.6988

Wang, D. D., Ou-Yang, L., Xie, H., Zhu, M., & Yan, H. (2020). Predicting the impacts of mutations on protein-ligand binding affinity based on molecular dynamics simulations and machine learning methods. *Computational and Structural Biotechnology Journal*, *18*, 439–454. https://doi.org/10.1016/j.csbj.2020.02.007

Wei, C., Bajpai, R., Sharma, H., Heitmeier, M., Jain, A. D., Matulis, S. M., Nooka, A. K., Mishra, R. K., Hruz, P. W., Schiltz, G. E., & Shanmugam, M. (2017). Development of GLUT4-selective antagonists for multiple myeloma therapy. *European Journal of Medicinal Chemistry*, *139*, 573–586. https://doi.org/10.1016/j.ejmech.2017.08.029

Yuan, Y., Kong, F., Xu, H., Zhu, A., Yan, N., & Yan, C. (2022). Cryo-EM structure of human glucose transporter GLUT4. *Nature Communications*, *13*(2671). https://doi.org/10.1038/s41467-022-30235-5

Zhao, X., An, X., Yang, C., Sun, W., Ji, H., & Lian, F. (2023). The crucial role and mechanism of insulin resistance in metabolic disease. *Frontiers in Endocrinology*, *14*(1149239). https://doi.org/10.3389/fendo.2023.1149239

Zhong, X., He, X., Wang, Y., Hu, Z., Huang, H., Zhao, S., Wei, P., & Li, D. (2022). Warburg effect in colorectal cancer: the emerging roles in tumor microenvironment and therapeutic implications. *Journal of Hematology and Oncology*, *15*(160). https://doi.org/10.1186/s13045-022-01358-5

Zhou, Q., Yang, X., Xiong, M., Xu, X., Zhen, L., Chen, W., Wang, Y., Shen, J., Zhao, P., & Liu, Q. H. (2016). Chloroquine increases glucose

uptake via enhancing GLUT4 translocation and fusion with the plasma membrane in L6 cells. *Cellular Physiology and Biochemistry*, *38*(5), 2030–2040. https://doi.org/10.1159/000445562